Research Article | Vol. 26, No. 6 | 19 Mar 2018 | OPTICS EXPRESS 7528
Optics EXPRESS

Resolution limits of quantum ghost imaging

PAUL-ANTOINE MOREAU,[1] ERMES TONINELLI,[1] PETER A. MORRIS,[1] REUBEN S. ASPDEN,[1] THOMAS GREGORY,[1] GABRIEL SPALDING,[2] ROBERT W. BOYD,[1,3,4] AND MILES J. PADGETT[1,*]

[1]*School of Physics and Astronomy, University of Glasgow, G12 8QQ, UK*
[2]*Department of Physics, Illinois Wesleyan University, Bloomington, Illinois 61701, USA*
[3]*Department of Physics, University of Ottawa, Ottawa, Ontario, Canada*
[4]*The Institute of Optics and Department of Physics and Astronomy, University of Rochester, Rochester, NY 14627, USA*
[*]*miles.padgett@glasgow.ac.uk*

Abstract: Quantum ghost imaging uses photon pairs produced from parametric downconversion to enable an alternative method of image acquisition. Information from either one of the photons does not yield an image, but an image can be obtained by harnessing the correlations between them. Here we present an examination of the resolution limits of such ghost imaging systems. In both conventional imaging and quantum ghost imaging the resolution of the image is limited by the point-spread function of the optics associated with the spatially resolving detector. However, whereas in conventional imaging systems the resolution is limited only by this point spread function, in ghost imaging we show that the resolution can be further degraded by reducing the strength of the spatial correlations inherent in the downconversion process.

OCIS codes: (270.0270) Quantum optics; (270.5290) Photon statistics; (110.0110) Imaging systems.

References and links

1. T. Pittman, Y. Shih, D. Strekalov, and A. Sergienko, "Optical imaging by means of two-photon quantum entanglement," Phys. Rev. A **52**, R3429 (1995).
2. D. Strekalov, A. Sergienko, D. Klyshko, and Y. Shih, "Observation of two-photon 'ghost' interference and diffraction," Phys. Rev. Lett. **74**, 3600 (1995).
3. E. d. S. Fonseca, P. S. Ribeiro, S. Pádua, and C. Monken, "Quantum interference by a nonlocal double slit," Phys. Rev. A **60**, 1530 (1999).
4. A. Gatti, E. Brambilla, and L. Lugiato, "Entangled imaging and wave-particle duality: from the microscopic to the macroscopic realm," Phys. Rev. Lett. **90**, 133603 (2003).
5. R. S. Bennink, S. J. Bentley, R. W. Boyd, and J. C. Howell, "Quantum and classical coincidence imaging," Phys. Rev. Lett. **92**, 033601 (2004).
6. O. S. Magaña-Loaiza, G. A. Howland, M. Malik, J. C. Howell, and R. W. Boyd, "Compressive object tracking using entangled photons," Appl. Phys. Lett. **102**, 231104 (2013).
7. P. A. Morris, R. S. Aspden, J. E. Bell, R. W. Boyd, and M. J. Padgett, "Imaging with a small number of photons," Nat. Commun. **6** (2015).
8. R. S. Aspden, N. R. Gemmell, P. A. Morris, D. S. Tasca, L. Mertens, M. G. Tanner, R. A. Kirkwood, A. Ruggeri, A. Tosi, R. W. Boyd, G. S. Buller, R. H. Hadfield, and M. J. Padgett, "Photon-sparse microscopy: visible light imaging using infrared illumination," Optica **2**, 1049–1052 (2015).
9. J. C. Howell, R. S. Bennink, S. J. Bentley, and R. Boyd, "Realization of the einstein-podolsky-rosen paradox using momentum-and position-entangled photons from spontaneous parametric down conversion," Phys. Rev. Lett. **92**, 210403 (2004).
10. R. S. Aspden, D. S. Tasca, R. W. Boyd, and M. J. Padgett, "Epr-based ghost imaging using a single-photon-sensitive camera," New J. Phys. **15**, 073032 (2013).
11. M. D'Angelo, A. Valencia, M. H. Rubin, and Y. Shih, "Resolution of quantum and classical ghost imaging," Phys. Rev. A **72**, 013810 (2005).
12. D. Tasca, R. Aspden, P. Morris, G. Anderson, R. Boyd, and M. Padgett, "The influence of non-imaging detector design on heralded ghost-imaging and ghost-diffraction examined using a triggered iccd camera," Opt. express **21**, 30460–30473 (2013).
13. R. S. Aspden, M. J. Padgett, and G. C. Spalding, "Video recording true single-photon double-slit interference," Am. J. Phys. **84**, 671–677 (2016).

#309547 https://doi.org/10.1364/OE.26.007528
Journal © 2018 Received 30 Oct 2017; revised 10 Feb 2018; accepted 12 Feb 2018; published 15 Mar 2018

Optics EXPRESS

14. A. Gatti, E. Brambilla, M. Bache, and L. A. Lugiato, "Correlated imaging, quantum and classical," Phys. Rev. A **70**, 013802 (2004).
15. J. H. Shapiro and R. W. Boyd, "The physics of ghost imaging," Quantum Inf. Process. **11**, 949–993 (2012).
16. E. Brambilla, A. Gatti, M. Bache, and L. A. Lugiato, "Simultaneous near-field and far-field spatial quantum correlations in the high-gain regime of parametric down-conversion," Phys. Rev. A **69**, 023802 (2004).
17. C. Law and J. Eberly, "Analysis and interpretation of high transverse entanglement in optical parametric down conversion," Phys. Rev. Lett. **92**, 127903 (2004).
18. P.-A. Moreau, F. Devaux, and E. Lantz, "Einstein-podolsky-rosen paradox in twin images," Phys. Rev. Lett. **113**, 160401 (2014).
19. J. Schneeloch and J. C. Howell, "Introduction to the transverse spatial correlations in spontaneous parametric down-conversion through the biphoton birth zone," J. Opt. **18**, 053501 (2016).
20. N. B. Nill, "Conversion between sine wave and square wave spatial frequency response of an imaging system," Tech. rep., MITRE corp. (2001).
21. J. W. Coltman, "The specification of imaging properties by response to a sine wave input," J. Opt. Soc. Am. **44**, 468–471 (1954).
22. D. Klyshko, "A simple method of preparing pure states of the optical-field, a realization of the einstein, podolsky, rosen experiment and a demonstration of the complementarity principle," Usp. Fiz. Nauk **154**, 133–152 (1988).
23. R. S. Aspden, D. S. Tasca, A. Forbes, R. W. Boyd, and M. J. Padgett, "Experimental demonstration of klyshko's advanced-wave picture using a coincidence-count based, camera-enabled imaging system," J. Mod. Optic. **61**, 547–551 (2014).

1. Introduction

Quantum ghost imaging was first demonstrated by Shih and coworkers in 1995 [1, 2]. These demonstrations used photon pairs created by spontaneous parametric down-conversion (SPDC) to obtain an image, or a diffraction pattern, using photons that have never interacted with the object, correlated with photons that have but are detected with no spatial information [3–5]. So called 'quantum ghost imaging' has been widely researched and shown to be of particular interest in the following cases: (a) when imaging using very few photons [6, 7]; (b) when transferring image information between widely disparate illumination and observing wavelengths [8] and (c) when imaging in conjugate bases to both demonstrate and utilize quantum entanglement [9, 10]. The ghost-imaging technique is particularly appealing as it allows the object to be placed in an optical path that is isolated from the imaging detector.

An outstanding question to ask is how the resolution performance of ghost imaging compares with conventional imaging and thus whether ghost imaging has any resolution benefits beyond being an intriguing use of correlated fields [11]. Quantum ghost imaging relies upon the spatially correlated pairs of photons that can be produced through parametric down-conversion and directed into two separate optical arms. In one possible configuration of the ghost imaging technique, the object is placed in one arm of the down-conversion system and a single-pixel 'heralding' detector indicates when the photon is transmitted through this object. If the photon is transmitted then the signal from this heralding detector triggers a camera positioned in the other arm, which then detects the spatial position of the correlated photon. Hence, the image information is in essence recovered from the coincidence detection of the two photons [10].

2. Experimental setup and theory

In most ghost imaging systems, the single-pixel heralding detector has a large area such that it detects photons across the full field of view of the imaging system. To maximize the collection efficiency, the detector needs to be of sufficient size to couple many spatial modes, at least one mode for each independent pixel in the image [12]. We can directly compare the resolution of conventional imaging and ghost imaging by changing the position of the object within the system (see Fig. 1(a)). As noted above, when the object is placed in the arm of the heralding detector, i.e. not the arm containing the camera, the system is a ghost-imaging system. Alternatively, when the object is placed in the same arm as the camera, then the system is a conventional imaging system, albeit one in which the camera is triggered using the heralding detector. In both configurations,

Optics EXPRESS

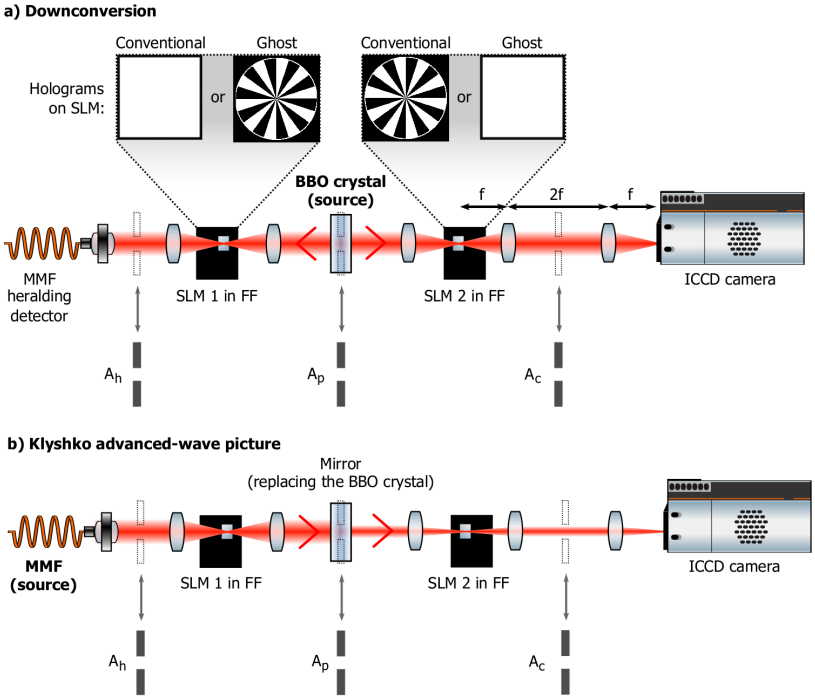

Fig. 1. (a) Simplified schematic of the down-conversion imaging system. The SLMs, either of which can be programmed to create the object (i.e. resolution target), are in the far-field (FF) of the BBO crystal. Depending upon which SLM is used to display the target, the configuration is either a conventional or ghost imaging system. The signal from the heralding detector coupled to a multimode fibre (MMF) triggers the ICCD camera. Three apertures A_c, A_p and A_h can be introduced respectively in the camera arm, in the pump and in the heralding arm. (b) The Klyshko Advanced Wave Picture. In this representation, the heralding detector is replaced by a classical source propagating through the system. The BBO crystal acts here as a mirror combined with a spatial filter of the same diameter as the pump beam in the down-conversion setup. Therefore, only a fraction of the beam scattered from the ghost object passes through the system, thereby limiting the resolution of the system.

we trigger the camera only when a photon is expected to be present; this temporal selectivity has the effect of suppressing background noise from the camera, thereby enabling ultra-low-light imaging [6, 7, 13].

In this paper, we directly examine the image resolution obtained in both conventional-imaging and ghost-imaging configurations (see Fig. 1(a)). We show that in both imaging systems the point-spread function of the camera optics sets a limit on the resolution of the acquired image. In heralded imaging, the resolution of the image is set solely by this limit. However, in ghost imaging, the situation is more complicated. Ultimately the resolution of a ghost imaging system cannot exceed the resolution with which the spatial correlations between the photons are created or measured [14, 15]. The effective strength of this correlation is therefore limited by a combination of a) the underlying strength of the spatial correlations b) the resolving power of the optics used to relay the downconversion crystal to the camera, c) the resolving power of the optics used to relay the crystal to the object.

A simplified schematic of the experiment configurations we use in the present work is shown in Fig. 1(a), in this unfolded representation the two photons are depicted as being emitted in opposite directions. This configuration is based on a previous setup presented and detailed in [13].

Optics EXPRESS

In summary, the system consists of a downconversion source, a single-pixel heralding detector in one arm and an intensified CCD (ICCD) camera in the other arm. As discussed above, the photons are highly correlated in transverse position and highly anti-correlated in transverse momentum. The photons are separated from each other into the two arms using a 50 : 50 pellicle beam splitter. In each arm, spatial light modulators (SLMs) are positioned in the far field of the source (i.e. in the back focal-plane of a transform lens) and are programmed to create a transmission object, in either of the two arms. In our present work, the object is a binary sector resolution target which allows the assessment of the resolution under different aperture sizes, object positions and various strengths of spatial correlation between the photons. In the heralding arm the photon is incident on the SLM that is itself imaged to the large-area, single-pixel, heralding detector. The heralding detector comprises a multi-mode fiber coupled to a single-photon avalanche detector (SPAD). The correlated photon is incident on the other SLM and is transmitted through a free-space, image-preserving, optical delay line before being imaged onto the ICCD camera. The optical delay line compensates for the electronic delays in the heralding detector and in the ICCD trigger electronics, ensuring that the photon reaches the camera at the precise moment that the camera is triggered by the heralding detector (i.e., establishing the $\approx$ 4ns coincidence window for all recorded measurements). In the ghost-imaging configuration the object is encoded onto the SLM in the heralding arm, whereas for the conventional imaging configuration the object is encoded onto the SLM in the camera arm (see Fig. 1(a)). In addition to the system as described above, various apertures can be inserted in the optical paths to restrict the numerical aperture of the optics and thereby lower the resolution with which various planes are re-imaged onto the camera. These apertures can be placed between the camera arm SLM and the camera, between the object arm SLM and the single-pixel detector, or placed in the pump beam to reduce its diameter. In all our configurations both the object and imaging detector are in the far-field of the crystal. Therefore, the position correlation inherent in the far-field of the crystal is determined by the anti-correlation of the transverse momenta of the signal and idler photons produced by the SPDC. The strength of this momentum anti-correlation is set by the transverse momentum uncertainty in the pump beam, which is itself controlled by its diameter. Consequently, as measured in the far-field, the position correlation radius between signal and idler photons is given as [16],

$$\sigma_x \approx f\frac{2\lambda_p}{\pi w_p} \tag{1}$$

where f is the effective focal length of the Fourier-transform lens and w_p is the waist of the pump beam. For our experimental configuration, and an unrestricted pump beam, this gives a correlation radius in the plane of the object of $\approx 100\mu$m (f = 100mm; $w_p \approx$ 0.45mm; λ_p = 355nm). Our conjecture is that irrespective of the resolving power of the optical system this correlation length sets a resolution limit that the ghost imaging system cannot exceed. Whereas the size of the pump beam potentially sets the resolution, the field of view of the imaging system is set due to the phase matching by the length of the crystal [16],

$$FOV_x \approx f\sqrt{\frac{\lambda_p}{L}} \tag{2}$$

and hence is not effected by any apertures placed in the pump beam. From the previous equations one can deduce a limit on the number of resolution cells for the ghost imaging system generated by the SPDC (i.e. the number of effective pixels).

$$V = \left(\frac{FOV_x}{\sigma_x}\right)^2 \approx \frac{\pi^2 w_p^2}{4L\lambda_p} \tag{3}$$

This number corresponds to the limit of the number of resolution cells in the ghost images due to the SPDC properties only, as we will see bellow the resolution can be further degraded by the optical setup used to acquire the images. V is also the Schmidt number of the entanglement [17,18].

Optics EXPRESS

Some of the confusion surrounding the resolution limits of ghost imaging possibly arise from the fact that the spatial correlation between signal and idler photons can be arbitrarily high. However, as we argue and show below, the practically realisable correlation length cannot be stronger than the resolution of the optical system used to measure it [19]. Therefore, in a ghost imaging system, what matters is the strength of the correlation between the photons as measured in the plane of the object with those measured in the plane of the image.

3. Evaluation of the modulation transfer function

In the following to assess the resolution of the different experimental systems we will evaluate the modulation transfer function (MTF) using binary spoke targets, we show here how it is done. The MTF is evaluated by converting the contrast transfer function (CTF) of the system extracted from the images of the binary spoke target. The CTF is the equivalent of the MTF evaluated with squared periodic waves rather that with sine waves [20]. It has been previously shown that it is possible to deduce the MTF from an evaluation of the CTF [21]. We follow here this method.

In order to evaluate the MTF we first evaluate the CTF for each of the images presented in Fig. 2. For that purpose we have created in each of the recorded images, several concentric circles with the centroid of the test target as their common center. The values of the various pixels lying on these circles were extracted and for each of the circles (ultimately, for a perfect imaging system, the pixel values change according to a square wave, of which the frequency is known), and the contrast of the resulting intensity variation along each circle was evaluated using the following expression:

$$C(r) = \frac{I_{max}(r) - I_{min}(r)}{I_{max}(r) + I_{min}(r)} \tag{4}$$

where r is the radius of the circle, $I_{max}(r)$ is the integrated intensity integrated on the dark spokes part of the resolution target, and $I_{min}(r)$ is the same quantity obtained on the bright spokes parts. As each radius r corresponds to a certain spatial frequency we can plot the contrast $C(\xi)$ as a function of the spatial frequencies which corresponds to the optical contrast transfer function of the imaging system.

Once the CTF $C(\xi)$ has been evaluated it can be converted into a MTF $M(\xi)$ by using Coltman's formula [21] :

$$M(\xi) = \frac{\pi}{4}\left[C(\xi) + \frac{C(3\xi)}{3} - \frac{C(5\xi)}{5} + \ldots\right] \tag{5}$$

In fact, it can be demonstrated that for frequencies greater than a third of the cut-off frequency only the first term contribute significantly to the MTF. In the context of the present work it has been verified that it is the case for any of the measured spatial frequencies. It means that in the present case the MTF is proportional to the evaluated CTF :

$$M(\xi) \approx \frac{\pi}{4} C(\xi) \tag{6}$$

The graphs of Fig. 3 have been obtained by using this method.

4. Results

We acquire both conventional and ghost images for varying size of apertures placed in far-field of the object in the camera arm A_c (Diameters $D_c = \{1.2\text{mm}; 0.9\text{mm}; 0.6\text{mm}\}$) with an effective focal $f_c = 150\text{mm}$ producing the fourier transform between the aperture plane and the plane of the object, the heralding arm A_h ($D_h = 4\text{mm}; 3\text{mm}; 2\text{mm}$) with an effective focal length $f_h = 500\text{mm}$ and the pump beam A_p ($D_p = 0.8\text{mm}; 0.6\text{mm}; 0.4\text{mm}$) with an effective focal length $f_p = 100\text{mm}$. The set of apertures in each plane has been chosen so that each of the three

Optics EXPRESS

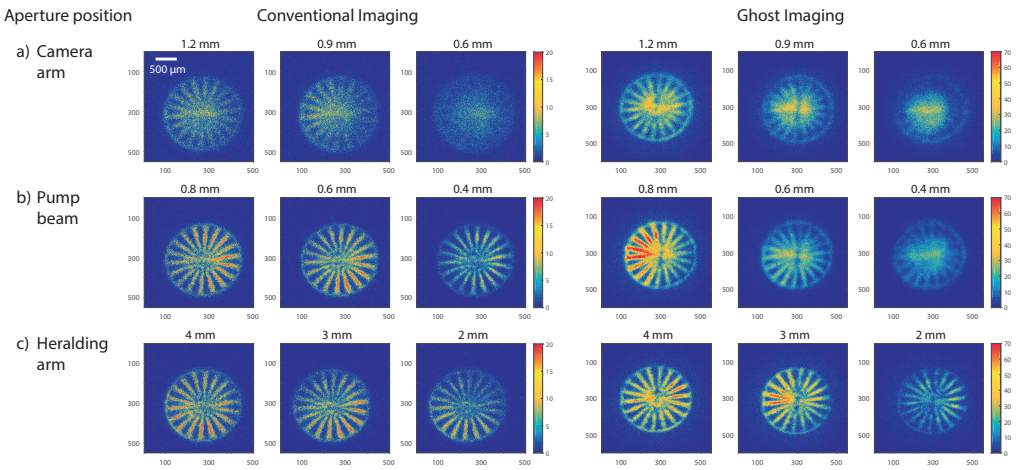

Fig. 2. Images of a binary sector resolution target acquired by summing 2000 binary frames of photon detection using conventional imaging and ghost Imaging for different apertures size placed in a) the camera arm; b) in the pump; c) in the heralding arm. The different apertures sizes in the same column correspond to equivalent resolution power. The $500\mu m$ white scale-bar shown at the top left also applies to all of the other reconstructed images shown in the figure. The colorbars are expressed in number of photons.

arms would have the same resolving power if the n^{th} aperture in each set was introduced in the three planes.

The images obtained in the different configurations are shown on Fig. 2. From these images, we have quantitatively studied the impact on the resolution of using apertures in the different positions: Fig. 3 shows an evaluation of the modulation transfer function (MTF) of the conventional and ghost imaging systems in a variety of scenarios derived from the images in Fig. 2. In each case the MTF is evaluated by converting the optical contrast transfer function [20, 21]. The method is detailed in the previous section.

We then compare our experimental results to different theoretical resolution limits associated to the different parts of the optical system. For that purpose, we have plotted dashed lines on Fig. 3 corresponding to the theoretical resolution limit set by the Rayleigh criterion. Practically, in each configuration there are three factors that can potentially limit the final resolution. The first one is the size of the aperture introduced in the system (red dashed line), the second one is the size of the pump (red dashed line) and the last one is the ultimate resolution of the camera arm (blue dashed line). On each plot, these three possible limit are shown and the actual limit in the experimental resolution in the different scenarios can be identified. For a particular dashed line associated with a limiting aperture of size D and used with an optical system producing the Fourier transform of effective focal length f, the Rayleigh criterion corresponds to a spatial frequency limit of $\nu \approx \frac{D}{1.22 f \lambda_{s/i}}$, where $\lambda_{s/i} = 2\lambda_p = 710$nm. The three dashed lines therefore correspond to this limit with different combinations of apertures and focal length. The red line corresponds to the aperture introduced in the system, in either the camera arm (Fig. 2(a) case: $D = D_c$ and $f = f_c = 150$mm) in the pump (Fig. 2(b) case: $D = D_p$ and $f = f_p = 100$mm) or in the Heralding arm (Fig. 2(c) case: $D = D_h$ and $f = f_h = 500$mm). The green dashed line that corresponds to size of the pump i.e. $D = 2w_p = 0.9$mm and $f = f_p = 100$mm. Finally, the blue dashed line corresponds to the ultimate resolution of the camera arm without extra introduced apertures, in which case it is limited by the aperture used to correctly filter the SLM diffraction orders ($D = 6$mm and $f = 500$mm).

When the aperture is placed in the camera arm (between the SLM and the camera) we see

Optics EXPRESS

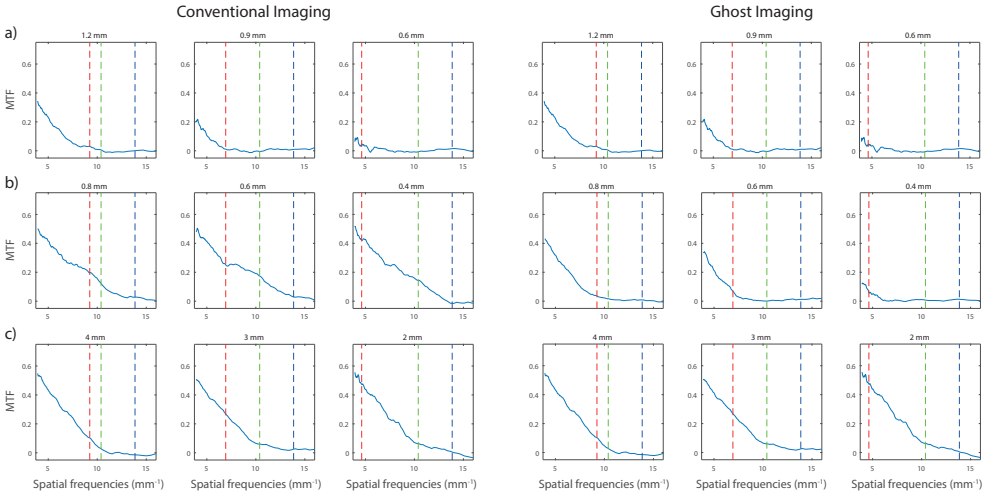

Fig. 3. Modulation transfer function of the imaging system, extracted from the images presented in Fig. 2, plotted as a function of the spatial frequencies of the object in the object plane for both conventional and Ghost imaging, and for apertures placed in a) the camera arm; b) in the pump; c) in the Heralding arm. The different dashed lines correspond to the expected resolution limits given by the Rayleigh criterion: the red one corresponds to the resolution limit set by the aperture placed in the different arms; the green one corresponds to the resolution limit set by the size of the unrestricted pump beam size; the blue corresponds to the resolution limit set by a camera imaging arm restricted only by the aperture used to correctly filter the SLM diffraction orders. In each graphs the ordinate corresponds to the MTF values (potentially varying from 0 to 1) and the abscissa corresponds to the spatial frequency associated with the size of the object features in its own plane.

that reducing its size degrades the resolution of the image (see Fig. 2(a)). Consistently it can be seen on Fig. 3(a) that in conventional and ghost configuration the resolution limit is given by the red dashed line (camera arm optical resolution limit set by the chosen aperture). In the conventional imaging case the degradation in resolution occurs because the reduction in the numerical aperture of the camera optics increases the size of the point spread function of the imaging optics. In the ghost-imaging configuration the point spread function limits the observed strength of the spatial correlation and hence the image resolution is similarly degraded.

When the aperture is placed in the heralding arm (between the SLM and the heralding detector) we see that reducing its size does not affect the resolution of the image, only its brightness (see Fig. 2(c)). Consistently it can be seen on Fig. 3(c) that the conventional imaging resolution is limited by the blue dashed line (unrestricted camera arm optical resolution limit) while the resolution limit of the ghost imaging is found around the green dashed line (unrestricted pump resolution limit). In the conventional imaging case this is because the reduction numerical aperture applies only to the heralding photon and not to the camera optics, as such it constitutes a source of loss in the heralding signal but does not affect the point-spread function of the camera optics. In the ghost-imaging case the aperture similarly restricts the numerical aperture of the large-area heralding detector but does not degrade the spatial correlation between the plane of the object and the plane of the camera.

When the aperture is placed in the pump beam we see that reducing its size makes no difference to the resolution of conventional imaging but does degrade the resolution of ghost imaging (see Fig. 2(b)). Consistently with the theoretical expectations, it can be seen on Fig. 3(b) that the conventional imaging resolution is limited by the blue dashed line (unrestricted camera arm

Optics EXPRESS

optical resolution limit) while the resolution limit of the ghost imaging is found around the red dashed line (pump aperture resolution limit). In the conventional imaging case this is because the reduction in pump beam size and hence spatial correlation of the photons does not change the point-spread function by which the object is imaged by the camera. In the ghost-imaging configuration, the reduction in pump beam size degrades the spatial correlation between the photon pairs and hence the image resolution is degraded.

The differences between conventional and ghost imaging can be alternatively understood using the Klyshko advanced wave picture (AWP) [22, 23], shown in Fig. 1(b). In the AWP the heralding detector is replaced with a classical source possessing the same characteristics of the heralding detector (aperture and numerical aperture) and this source backpropagates through the heralding arm to the nonlinear crystal. The front facet of the crystal acts as a mirror and reflects the light back into the camera arm. The intensity distribution measured by the camera is an exact prediction of that which would be detected by measuring the down-converted photons in coincidence with the heralding detector. As a consequence, in the AWP, when an aperture is introduced in the camera arm, because the aperture act as a spatial filter placed after the object the resolution is expected to be degraded whenever the object is placed in ghost of conventional configuration. This is compatible with the observations made on Fig. 2(a) and Fig. 3(a) where the resolution appears to be degraded in both configurations. Moreover, in the AWP, when an aperture is introduced in the heralding arm, it only filters spatially the illumination light wherever the object is placed and it has no substantive effect on the resolution of the image. This is compatible with the observations of Fig. 2(c) and Fig. 3(c), where no loss in terms of resolution is observed. Finally, in the AWP the aperture in the pump beam is analogous to a spatial filter mid way through the imaging system. When the object is positioned for conventional imaging this spatial filter acts only on the spatial mode of the illumination light and hence has no substantive effect on the resolution of the image. However, when the object is positioned for ghost imaging, the spatial filter lies between the object and the camera and hence reduces the resolution of the image. This is in agreement with the experimental results obtained and shown in Fig. 2(b) and Fig. 3(b), the resolution is degraded only in the Ghost imaging case. Note that in many previous configurations utilized for ghost imaging, including the comparison presented in [7], the heralded and ghost configurations have shown similar resolution. This similarity is most likely because the pump beam was large and thus the resolution of both heralded-imaging and ghost-imaging configuration was in both cases limited only by the resolving power of the optics between the crystal and the camera/object.

5. Conclusion

In the present work, we have compared the resolution of conventional and ghost imaging and discussed the influence of strength of the correlations produced by the down-conversion source and its effect on the image resolution. The experimental results obtained are in good agreement with the theoretical resolution limit as set by the Rayleigh criterion. We show that whilst in the case of conventional imaging, the resolution is largely independent of the source characteristics, in the ghost-imaging configuration the resolution of the resulting image is dependent on the strength of the correlations produced by the down-conversion source. Furthermore, in both the conventional and quantum cases the resolution of the image is limited by the point-spread function of the optics associated with the camera detector.

Funding

Engineering and Physical Sciences Research Council (EP/M01326X/1); European Research Council (TWISTS, 340507); European Union's Horizon 2020 Research and Innovation Programme (Marie Sklodowska-Curie grant agreement No 706410);

Optics EXPRESS

Acknowledgements

This work was funded by the UK EPSRC (QuantIC EP/M01326X/1) and the ERC (TWISTS, Grant no. 192382). P-AM acknowledges the support from the European Union's Horizon 2020 research and innovation programme under the Marie Sklodowska-Curie grant agreement No 706410. RMB gratefully acknowledges the support from the Canada Excellence Research Chairs program and the Natural Science and Engineering Research Council of Canada. ET acknowledges the financial support from the EPSRC Centre for Doctoral Training in Intelligent Sensing and Measurement (EP/L016753/1). T.G. acknowledges the financial support from the EPSRC (EP/N509668/1) and the Professor Jim Gatheral quantum technology studentship. PAM acknowledges the support from the UK EPSRC.

Disclosures

The authors declare that there are no conflicts of interest related to this article.